arXiv:1403.6935v2 [cond-mat.mtrl-sci] 3 Apr 2014

Hyperfine Clock Transitions of Bismuth Donors in Silicon Detected by Spin Dependent Recombination

P. A. Mortemousque,[1] S. Berger,[1,2] T. Sekiguchi,[1] C. Culan,[1] R. G. Elliman,[3] and K. M. Itoh[1]

[1] *School of Fundamental Science and Technology, Keio University, 3-14-1 Hiyoshi, Kohoku-ku, Yokohama 223-8522, Japan*

[2] *Department of Physics, ETH Zurich, CH-8093 Zurich, Switzerland*

[3] *Australian National University, Research School of Physics and Engineering, Canberra, ACT 0200, Australia*

Bismuth donors ion-implanted in ^{28}Si and $^{\mathrm{nat}}$Si are studied using magnetic resonance spectroscopy based on spin dependent recombination. The hyperfine clock transition, at which the linewidth is significantly narrowed, is observed for the bismuth donors. The experimental results are modeled quantitatively by molecular orbital theory for a coupled pair consisting of a bismuth donor and a spin dependent recombination readout center, including the effect of hyperfine and Zeeman interactions.

I. INTRODUCTION

Among a variety of physical systems investigated for quantum information processing, superconducting qubits are one of the promising candidates as quantum processors because of their fast operation capabilities and their potential for scalability.[1] However, because of their relatively fast decoherence rate which might be insufficient for maintaining quantum information throughout the course of computation, development of quantum memories that could support the operation of the superconducting processors are desired. Such memory qubits have to be addressable at low magnetic field (< 10 mT for aluminum[2]), since superconducting qubits become unoperable at magnetic fields higher than their critical fields.

Within this context, a bismuth (Bi) donor in silicon (Si) has attracted much attention recently. Its large hyperfine interaction $A = 1.4754$ GHz (Ref. 3) and the ^{209}Bi nuclear spin $I = 9/2$ give rise to a large zero-field splitting of 7.4 GHz that is comparable to the typical energy splitting between $|R\rangle$ and $|L\rangle$ states of superconducting flux qubits.[4] Thus, coherent coupling between a Bi spin qubit in Si and a superconducting flux qubit on Si is in principle possible via a microwave photon traveling through a waveguide placed between the two qubits.[5,6] The proposal to couple Bi in Si with a superconducting qubit[6] have triggered extensive fundamental studies of the Bi donor in Si very recently. Starting from the spectroscopic analysis of the electron paramagnetic resonance (EPR),[6,7] the electron spin relaxation time T_1,[5,8] decoherence time T_2,[5,7–10] and superhyperfine interaction with nearby ^{29}Si nuclear spins[8,11] were investigated. Moreover, the coherent coupling between the Bi electrons and ^{209}Bi nuclear spins[6] and dynamic nuclear polarization of ^{209}Bi were achieved.[5,12] Hybrid nuclear-electronic qubits consisting of superpositions of electronic and nuclear spin states have been used to demonstrate five orders of magnitude longer coherence times than the manipulation times.[13] In order to extend the coherence time of Bi donor electrons, magnetic field-insensitive clock transitions can be used.[10,11,14] Also, at low temperatures, the presence of 4.7% ^{29}Si (I=1/2) in naturally available silicon ($^{\mathrm{nat}}$Si) limits the coherence time of donors[15,16] so that the use of isotopically purified ^{28}Si is helpful.[10,17,18] The fact that most of aforementioned Si:Bi studies were performed in the past three years shows how rapidly developing this field is. However, one aspect that has been scarcely studied is the investigation of Si:Bi at low-fields to enable the coupling to superconducting qubits. In order to fill in this gap, we have shown recently[19] that magnetic resonance spectroscopy with detection based on spin dependent recombination[20] (SDR) allows to manipulate and detect spins at low magnetic fields.

In the present study, using such a capable SDR technique, we perform spectroscopy of bismuth implanted in both $^{\mathrm{nat}}$Si and isotopically enriched ^{28}Si samples and observe a significant line narrowing at the hyperfine clock transition (HCT), where the transition frequency ν is insensitive to the change in A induced by variations in charge distribution ($\partial\nu/\partial A = 0$). While existence of optimal working points (e. g., gate voltages) at which superconducting qubits are immune to the electric charge noise has been demonstrated,[21] observation of HCT in solid state systems has never been reported to our knowledge. The HCT is different from the conventional clock transition, which is insensitive to magnetic noise ($\partial\nu/\partial B_z = 0$). The conventional clock transitions are routinely employed in the operation of atomic clocks[22,23] utilizing ^{133}Cs and trapped ions.[24] A similar clock transition of bismuth donors in silicon has been adopted to achieve extremely long donor electron spin coherence time.[10] HCT investigated in this study is more involved in the sense that the hyperfine interaction of a donor can be affected by both strain and electric field fluctuations. Away from the HCT point, the interaction of a donor (D) electron with a nearby implantation defect, which is used in SDR spectroscopy as a readout center (R), causes an asymmetric broadening of the spectral line shapes. This interaction is equivalent to an effective electric perturbation. Thus we propose a theoretical model that describes the change of the donor wave function due to the presence of this readout center. This model makes it possible to simulate the SDR spectra and estimate the associated change in the hyperfine interaction. Finally, we compare the line position and the line shape measured by SDR spectroscopy with our calcula-

tion and extend the theoretical model for other donors in silicon.

II. EXPERIMENTAL OBSERVATION OF THE CHANGE IN HYPERFINE INTERACTION

A. Samples

Two types of samples were employed; a silicon crystal enriched to 99.983% ^{28}Si ([^{29}Si] = 90 ppm and [^{30}Si] = 80 ppm) with a resistivity $\approx$ 10 Ω·cm and a highly resistive ($>$ 3 kΩ·cm) float-zone $^{\rm nat}$Si. These two substrates were ion-implanted with Bi and are labeled ^{28}Si:Bi and $^{\rm nat}$Si:Bi, respectively. The ion implantations were performed at room temperature with the total fluence of 2×10^{13} cm^{-2}. The implantation energies were 300 and 550 keV with the doses of 0.7×10^{13} and 1.3×10^{13} cm^{-2}, respectively. These conditions yielded a maximum bismuth concentration of 1.8×10^{18} cm^{-3} (above the solubility limit[25]) in the depth of 90 to 150 nm from the surface. The post-implantation annealing, performed at 650 °C for 30 min in an evacuated quartz tube, led to an activation efficiency[7,26–28] below 60%, resulting in the Bi donor concentration less than 1.1×10^{18} cm^{-3} (below the metal-insulator transition[29]). This process was designed to maximize the number of D-R pairs, instead of fully activating all the implanted Bi atoms.[30]

B. SDR method

The continuous illumination provided by a 100-W halogen lamp (above band-gap power of 100 mW/cm^2 outside the EPR cavity) generated photoexcited electrons in the sample. The capture of photocarriers by the ionized donors of D-R pairs takes place on a time scale τ_{ec} of the order of 10 to 100 μs for an illumination at 635 nm of 20 mW/cm^2 at 5 K.[31] For the phosphorus donor coupled to a dangling bond readout center, the expected recombination time for the antiparallel electron spin pair was typically $\tau_{\rm ap} \approx 10$ μs whereas for the parallel spin pair, the recombination time $\tau_{\rm p} \approx 1$ ms was much longer.[31] Preliminary time-resolved electrically detected magnetic resonance (EDMR) measurements of Bi-R pairs in $^{\rm nat}$Si:Bi showed a dynamics similar to the donor coupled to a dangling bond defect situating at the Si/SiO$_2$ interface even though the readout centers R created by the implantation were situated around 90 nm deep Bi donors. As a consequence, only the parallel spin pairs remained in the steady state under illumination without external induction of the magnetic resonance. Therefore, flipping the donor electron spins by the external magnetic resonance irradiation broke this steady-state constant current situation and decreased the photocurrent by the enhancement of the spin-dependent recombinations.[20] Such a change of the sample photoconductivity led to a decrease in the absorption of the microwave electric field by the sample (photocarriers) leading to an enhancement in the Q factor of the EPR cavity. The defect utilized as a readout center in this study had a g factor of $g \approx 2.005$ measured by the cross-relaxation R($|1\rangle \leftrightarrow |2\rangle$)-Bi($|8\rangle \leftrightarrow |13\rangle$) (Ref. 19) but its microstructure was unknown. In our measurement, the sample was placed in the JEOL JES-RE3X X band EPR spectrometer. A small coil placed near the sample within the EPR cavity was used to excite the magnetic resonance. On the other hand, the X-band ($\approx$ 9.08 GHz) irradiation and reflection were used for probing the change in the sample conductivity. Since the additional coil near the sample could apply an arbitrary microwave frequency, it was possible to reduce the frequency along with the static magnetic field.[19] The second derivative of the reflected X-band intensity with respect to the field modulation was recorded as an SDR signal to reduce the broad cyclotron resonance lines and the background change of the sample conductivity during the magnetic field scan. All the SDR measurements were performed at 16 K.

C. Experimental results

The Bi donor can be modeled by the spin Hamiltonian

$$\mathcal{H}_1 = g_e \mu_B B_z S_z - g_n \mu_N B_z I_z + hA\mathbf{S} \cdot \mathbf{I}, \qquad (1)$$

where g_e and g_n are the donor electron and nuclear g-factors, respectively, and A the value of the isotropic hyperfine interaction in units of frequency. We label the i-th eigenstate in order of increasing energy as $|i\rangle$. The Breit-Rabi diagram of the bismuth donor is shown in Fig. 1(a). The Hamiltonian parameters used are summarized in Table I, together with the ones extracted from the SDR data of this study. The sensitivity of the resonant magnetic field to a parameter p for a given resonant frequency ν is defined as $\delta B_z/\delta p$, which satisfies

$$\delta\nu = \frac{\partial \nu}{\partial p}\delta p + \frac{\partial \nu}{\partial B_z}\delta B_z = 0 \qquad (2)$$

which leads to $\partial\nu/\partial A = -(\partial\nu/\partial B_z)(\delta B_z/\delta A)$. For $\partial\nu/\partial A$ to be zero, $\delta B_z/\delta A$ must be zero since when $\partial\nu/\partial B_z = 0$, $\delta A = 0$ (Ref. 10) so that $\partial\nu/\partial A$ takes a finite value.

Figures 1(b–d) and 1(e–g) show cw SDR spectra of $^{\rm nat}$Si:Bi and ^{28}Si:Bi. The spectra recorded at the Bi donor HCT for $m_I = -7/2$ (7.3043 GHz for $^{\rm nat}$Si:Bi and 7.3054 GHz for ^{28}Si:Bi) between the states $|9\rangle$ and $|12\rangle$ [Figs. 1(c, f)] have a symmetric line shape whereas the X-band spectra of the $|1\rangle \leftrightarrow |20\rangle$ transition ($m_I = 9/2$) and the $|10\rangle \leftrightarrow |11\rangle$ transition ($m_I = -9/2$), shown in Figs. 1(b, e) and in Figs. 1(d, g), respectively, are asymmetric. At the HCT, the resonant field sensitivity to the hyperfine value $\delta B_z/\delta A$ is zero so that one can probe the Si:Bi linewidth and line shape not subject to such electric perturbations. The measured FWHM linewidth of the HCT lines are 6.7 G and 1.3 G for $^{\rm nat}$Si:Bi and for ^{28}Si:Bi, respectively. These values are significantly larger than the

measured linewidth at X-band of 4.1 G for ^{nat}Si:Bi[5,6] and the theoretical prediction of 0.08 G at the HCT$_{9-12}$ for ^{28}Si:Bi.[9] In contrast, the X-band $|1\rangle \leftrightarrow |20\rangle$ transitions are asymmetrically broadened (FWHM linewidths of 7.7 G and 1.6 G) toward high field and the $|10\rangle \leftrightarrow |11\rangle$ transitions toward low field (7.0 G and 1.4 G). m_I dependent asymmetry directions can be described by an (inhomogeneous) distribution of the hyperfine interaction but is inconsistent with any distribution of the Zeeman interaction.

Let us now discuss whether the experimental conditions we employed are sufficient to achieve the intrinsic linewidth and shape of the Bi donor spin transitions. In the duration of a single measurement, the microwave frequency of the EPR spectrometer drifts typically by ± 5 kHz. The signal generated at 7 GHz by an Agilent 8257D microwave source in series with a 3-W MiniCircuits ZVE-8G+ amplifier exhibits a frequency stability of ± 1.5 kHz for the same duration. These fluctuations in the applied microwaves lead to a maximum line broadening of $\pm 2.5 \times 10^{-3}$ G at 9 GHz and $\pm 1 \times 10^{-3}$ G at 7 GHz, which is negligibly small compared to the estimated $\gtrsim 10^{-2}$ G precision in magnetic field and its inhomogeneity.

The asymmetric line broadening of the $|1\rangle \leftrightarrow |20\rangle$ and $|10\rangle \leftrightarrow |11\rangle$ transitions is consistent with a distribution of the donor hyperfine interactions with a long tail toward low hyperfine couplings. From the line shapes of the spectra in Figs. 1 (b, d, e and g), the asymmetric part of the line broadening can be estimated roughly 1 G, corresponding to a distribution of the hyperfine constant A toward lower values by 3 MHz. We can exclude the distribution in the donor g-factor as a cause of this asymmetric broadening, because the sensitivity $\delta B_z/\delta g_e$ is negative for both transitions so that the broadening for both $|1\rangle \leftrightarrow |20\rangle$ and $|10\rangle \leftrightarrow |11\rangle$ transitions would be in the same direction. The spin exchange interaction $J\,\boldsymbol{S}_D \cdot \boldsymbol{S}_R$ (Ref. 32) between the two electrons of the SDR pair can also be ruled out as it would yield a symmetric line broadening for low enough couplings, estimated by Lu *et al.*[33] to be below 5 MHz for phosphorus donor coupled to a surface dangling bond (^{31}P$-$P$_{b0}$) and below 10 kHz for separations larger than one donor Bohr radius

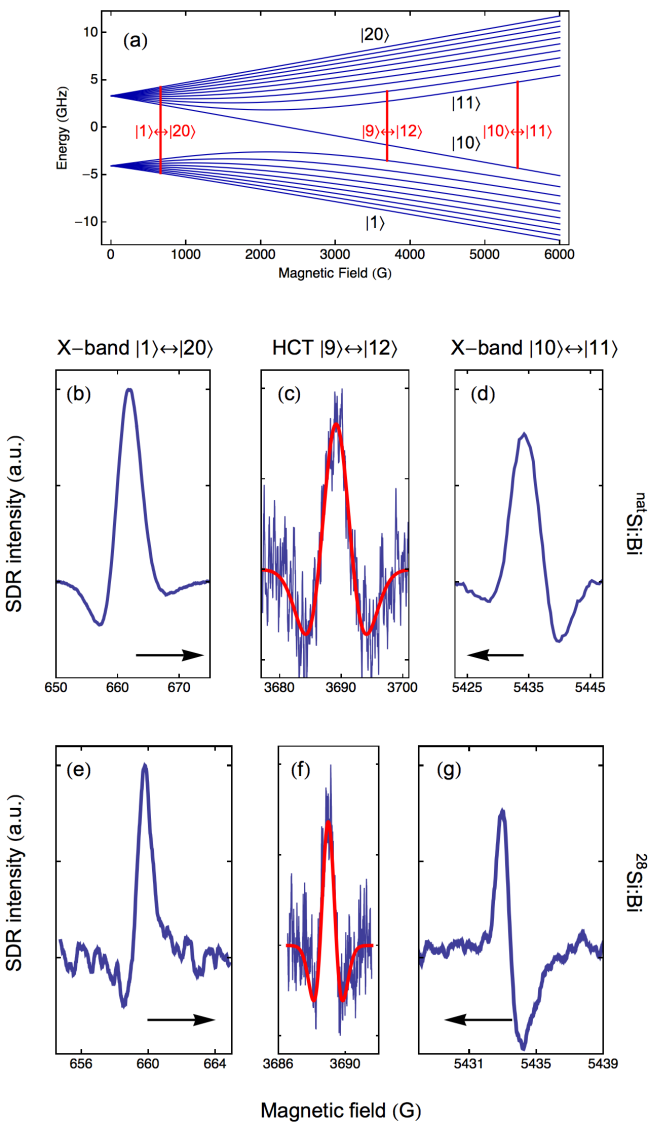

FIG. 1. (Color online.) (a) Breit-Rabi diagram of the bismuth donor spins. The three vertical red lines correspond to the transitions shown in (b−g). cw SDR spectra of ^{nat}Si:Bi (b−d) and ^{28}Si:Bi (e−g). The FWHM linewidths of the HCT$_{9-12}$ (c) and (f), obtained from the double integration of the fitting Gaussians (red lines), are 6.7 G for ^{nat}Si:Bi and is 1.3 G for ^{28}Si:Bi. Arrows indicate the direction of the asymmetric broadening directions. The signal-to-noise (S/N) ratios for $|9\rangle \leftrightarrow |12\rangle$ are worse than the others since the HCT$_{9-12}$ line intensity for Si:Bi is much weaker than the intensities for the X-band $|1\rangle \leftrightarrow |20\rangle$ and $|10\rangle \leftrightarrow |11\rangle$ lines as will be shown theoretically in Fig. 7.

TABLE I. Magnetic resonance parameters of ^{28}Si:Bi and ^{nat}Si:Bi. The fractional changes in g-factor and in hyperfine interaction, are calculated as $(g_e^{SDR} - g_e^{EPR})/g_e^{EPR}$ and $(A^{SDR} - A^{EPR})/A^{EPR}$. The values for SDR[b,c] i.e., A^{SDR} (b, c) and g_e^{SDR} (c) are obtained from the fitting of the SDR peak positions by Eq. (1), assuming Gaussian distributed resonance peaks.

^{28}Si:Bi	g_e	$\Delta g_e/g_e$ (ppm)	g_n	A (MHz)	$\Delta A/A$ (ppm)
EPR[a]	2.00032	Ref.	0.9135	1475.17	Ref.
SDR[b]	2.00036(4)	+19(22)		1475.31(7)	+95(50)
SDR[c]	2.00038(2)	+29(10)		1475.29(7)	+84(50)
^{nat}Si:Bi					
EPR[de]	2.0003	Ref.	0.914	1475.4	Ref.
SDR[c]	2.00049(5)	+93(25)		1475.05(17)	−240(120)

[a] Wolfowicz *et al.* (Ref. 10)
[b] g-factor and A fitting parameters.
[c] g-factor determined at HCT$_{9-12}$, A used as fitting parameter
[d] Feher (Ref. 3)
[e] Morley *et al.* (Ref. 5)

a_B.[34] The values of $|\delta B_z/\delta J|$, $\delta B_z/\delta A$ and $\delta B_z/\delta g_e$ corresponding to each spectrum in Fig. 1 are summarized in Table II.

Other possible causes for the observed asymmetric broadening would be the strain induced by the implantation damage that was not recovered fully by the post-implantation annealing process.[35] For shallow donors (P, As, Sb) in silicon, Wilson and Feher[36] and Dreher *et al.*[37] have shown that uniaxial macroscopic strain decreases the hyperfine interaction mainly through the valley repopulation of the ground-state Bloch function. Recently, Dreher (Ref. 38) has shown that, despite the fact that Bi has a large electron binding energy of 71 meV, the strain decreases its hyperfine interaction in the manner similar to other shallow donors. However, the effective hyperfine of the Bi donors in ^{28}Si, obtained from the peak positions in the SDR spectra, is +84 ppm higher than the reported value for EPR measurements.[10] Thus the macroscopic strain cannot account for the observed positive shift in effective hyperfine interaction. In fact, the positive shift suggests that orbitals of the donor and the readout center electrons are coupled and their densities are redistributed. In this study, we thus describe the SDR pair in terms of a model based on the coupling between the electron orbitals of the pair in this study.

III. CALCULATION OF THE LINE SHAPE WITH THE SDR MODEL

One Bi donor electron and one readout center electron form a spin pair. In section III A, we introduce a theoretical model to describe this electron pair. Then, we evaluate the effect of the readout center on the donor hyperfine properties (section III B) and we discuss the influence of the model parameters on the line shape (section III C).

A. wave function of the donor-readout center pair

The one-electron molecular orbitals corresponding to the neutral donor in the presence of an ionized readout center (D^0-R^+) and to a neutral readout center close to an ionized donor (D^+-R^0) are denoted by ϕ_D and ϕ_R, respectively. In a simplified picture, ϕ_D and ϕ_R can be expressed as a linear combination of the wave functions of the electron of an isolated donor χ_D and an isolated center χ_R so that $\phi_D = a_1\chi_D + a_2\chi_R$ and $\phi_R = b_1\chi_D + b_2\chi_R$. The linear coefficients $a_{1,2}$ and $b_{1,2}$ are calculated by applying the variational method to the one-electron Hamiltonian $\mathcal{H}_0 = K^* + V_D^* + V_R^*$ where K^* is the effective kinetic energy of the electron, V_D^* is the screened Coulomb potential of the donor, and V_R^* is the effective potential of the readout center. The difference in energy between these molecular states ϕ_i and the isolated states χ_i is small, even for a small spatial separation. This is due to the significant difference in the two orbitals χ_D and χ_R. The electron densities $|\chi_D|^2$ and $|\chi_R|^2$ are plotted in Fig. 2(a), and those of the one-electron molecular orbitals $|\phi_D|^2$ and $|\phi_R|^2$ in Fig. 2(b).

Antisymmetrized wave functions of the two-electron system, including the spin part, are constructed using the Slater determinant of the one-electron molecular orbitals:

$$\psi_1 = \phi_R\ \phi_R\,|0,0\rangle \otimes |m_I\rangle \tag{3a}$$
$$\psi_+ = 2^{-1/2}\left(\phi_D\ \phi_R + \phi_R\ \phi_D\right)|0,0\rangle \otimes |m_I\rangle \tag{3b}$$
$$\psi_- = 2^{-1/2}\left(\phi_D\ \phi_R - \phi_R\ \phi_D\right)|1,m_\sigma\rangle \otimes |m_I\rangle \tag{3c}$$
$$\psi_4 = \phi_D\ \phi_D\,|0,0\rangle \otimes |m_I\rangle\,. \tag{3d}$$

In the above, the spin states are denoted as $|\sigma, m_\sigma\rangle$ with $\sigma = S_D \pm S_R$ and the orbital products of the ϕ_i correspond, from left to right, to the first and the second electrons of the system. One notices that the spin singlet state ψ_+ (triplet ψ_-) behaves like a bonding (antibonding) orbital. Note that these states correspond to the charge states D^+–R^-, D^0–R^0 (σ=0), D^0–R^0 (σ=1) and D^-–R^+, respectively.

Furthermore, the charge repulsion $1/r_{12}$ can be included. The corrected two-electron molecular orbitals Ψ_i are then written as linear combinations of ψ_i. Thus, the bonding orbital is $\Psi_+ = N_+^{-1}(\psi_+ + c_1\psi_1 + c_4\psi_4)$, where the coefficients are $c_1 = \frac{\langle\psi_1|1/r_{12}|\psi_+\rangle}{E_+ - E_1}$ and $c_4 = \frac{\langle\psi_4|1/r_{12}|\psi_+\rangle}{E_+ - E_4}$. Then, assuming a negatively charged

TABLE II. The resonant field (B_z) sensitivity to the g-factor g_e and to the hyperfine A for the Si:Bi transitions shown in Fig. 1. m_I represents the nuclear spin projection of the EPR transitions but is not a good quantum number for all these levels, expect for $|10\rangle$ and $|20\rangle$. The calculation was performed using the EPR magnetic resonance parameters shown in Table I.

Transition (spectrum in Fig. 1)	m_I	$\lvert\delta B_z/\delta J\rvert$ [G/MHz]	$\delta B_z/\delta g_e$ [10^3 G]	$\delta B_z/\delta A$ [G/MHz]
$\lvert1\rangle \leftrightarrow \lvert20\rangle$ (b, e)	9/2	0.08	−0.3	−1.9
$\lvert9\rangle \leftrightarrow \lvert12\rangle$ (c, f)	−7/2	0.06	−1.8	0
$\lvert10\rangle \leftrightarrow \lvert11\rangle$ (d, g)	−9/2	0.08	−2.7	1.4

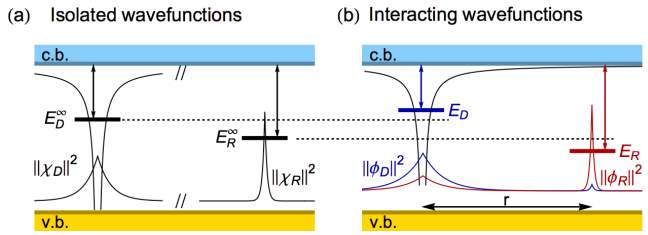

FIG. 2. (Color online.) Energy diagrams of the donor and readout center in the silicon band gap for the isolated states (a) and for the molecular orbitals (b). The corresponding electron densities are also plotted, together with the Coulomb potential of the ionized donor.

donor (D^-) with an energy $\approx E_4 \gg E_+, E_1$, the coefficient c_4 tends to zero and the contribution of ψ_4 to Ψ_+ can be neglected. It follows that

$$\Psi_+ = N_+^{-1}\Big(\psi_+ + c_1\psi_1\Big). \tag{4}$$

In the coefficient c_1, the term $\langle\psi_1|1/r_{12}|\psi_+\rangle$ can be approximated as $\approx \sqrt{2}\,\theta\,E_{\rm corr}$ where $E_{\rm corr}$ is the two-electron correlation energy taken as the Coulomb repulsion of the electrons in the R^- state. In this model, $E_{\rm corr}$ is included in the parameter $\epsilon_{\rm corr} = E_{\rm corr}/(E_+ - E_1) \approx E_{\rm corr}/(E_+ - E_{R-})$. On the other hand, the antibonding spin triplet state ψ_- does not mix with either of the spin singlet states $\psi_{1,+,4}$, i. e., we have $\Psi_- = \psi_-$.

B. Change in hyperfine interaction

The Fermi hyperfine interaction for the two electrons is

$$\mathcal{H}_{\rm hyp} = -\frac{2}{3}\,\mu_0\;\boldsymbol{\mu}_{\rm Bi}\cdot\sum_{i=1}^{2}\boldsymbol{\mu}_i\rho_i(\boldsymbol{r}_{\rm Bi}), \tag{5}$$

where $\rho_i(\boldsymbol{r}_{\rm Bi})$ is the one-electron density at the bismuth nucleus. The electron magnetic dipolar moment $\boldsymbol{\mu}_i$ depends on the electron orbital function. As the two-electron orbitals can be expressed as functions of χ_D and χ_R, only two operators $\boldsymbol{\mu}_D = -g_D\,\mu_B\boldsymbol{S}_D$ and $\boldsymbol{\mu}_R = -g_R\,\mu_B\boldsymbol{S}_R$ are relevant, where g_D and g_R are the g-factors of the isolated donor and readout center electrons, respectively. In order to simulate the SDR line shape, we only consider the change in the electron distribution while assuming the g-factor of the isolated centers. However, due to the confined nature of the readout center, only the χ_D component has a significant electron density at the bismuth nucleus. Then, in the rest of this section, the subscript of ρ_D is dropped.

Now, if one considers the hyperfine interaction A_{m_R} for a given spin projection m_R of the readout center, one finds that

$$\langle m_R = 1/2|\mathcal{H}_{\rm hyp}|m_R = 1/2\rangle = \begin{pmatrix}\mathcal{A}_{p,p} & \mathcal{A}_{p,ap}\\ \mathcal{A}_{ap,p} & \mathcal{A}_{ap,ap}\end{pmatrix} \tag{6}$$

$$\langle m_R = -1/2|\mathcal{H}_{\rm hyp}|m_R = -1/2\rangle = \begin{pmatrix}\mathcal{A}_{ap,ap} & \mathcal{A}_{p,ap}\\ \mathcal{A}_{ap,p} & \mathcal{A}_{p,p}\end{pmatrix} \tag{7}$$

where each $\mathcal{A}_{j,k}$ on the right-hand side is a block matrix of dimension $2I+1$, calculated using the electron density $\rho_{j,k}$ with subscripts indicating the parallel and antiparallel electron spin configurations: $\mathcal{A}_{p,p} = \langle\Psi_-|\mathcal{H}_{\rm hyp}|\Psi_-\rangle$, $\mathcal{A}_{p,ap} = \langle\Psi_-|\mathcal{H}_{\rm hyp}|(\Psi_- - \Psi_+)/\sqrt{2}\rangle = \langle\Psi_-|\mathcal{H}_{\rm hyp}|(\Psi_- + \Psi_+)/\sqrt{2}\rangle$ and $\mathcal{A}_{ap,ap} = \langle(\Psi_- - \Psi_+)/\sqrt{2}|\mathcal{H}_{\rm hyp}|(\Psi_- - \Psi_+)/\sqrt{2}\rangle = \langle(\Psi_- + \Psi_+)/\sqrt{2}|\mathcal{H}_{\rm hyp}|(\Psi_- + \Psi_+)/\sqrt{2}\rangle$. On the other hand, the off-diagonal blocks $\langle m'_R|\mathcal{H}_{\rm hyp}|m_R\rangle$ for $m'_R \neq m_R$ give a contribution only at the second and higher orders, which are neglected in this model. The simulation of the fractional change in the electron density at the donor nucleus $\Delta\rho/\rho_0$ was performed using a single exponential envelope function characterized by the Bohr radius $a_B = 8.1$ Å for the Bi donor electron and a Dirac function for the readout center. $\Delta\rho/\rho_0$ is plotted in Fig. 3 for a readout center energy of -0.55 eV, and repulsion energy parameters $\epsilon_{\rm corr} = 0$ (a) and $\epsilon_{\rm corr} = 0.5$ (b). One notices that a large repulsion energy parameter decreases the hyperfine interaction for the electron spin pair in the triplet configuration.

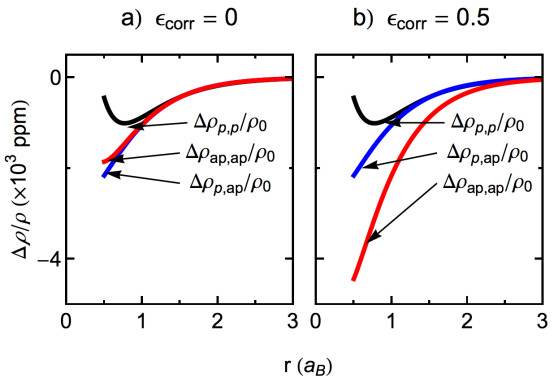

FIG. 3. (Color online.) Fractional changes in the electron density ρ for three different electron spins configurations plotted as a function of the separation r between the donor and the readout center in units of a_B. ρ_0 corresponds to the isolated bismuth donor. A typical fractional change of -2×10^3 ppm corresponds to a change of the Bi hyperfine interaction of -3 MHz.

C. SDR model parameters

The present model contains three physical parameters for a given donor in silicon: the concentration of readout centers N_R, and two parameters E_R and $\epsilon_{\rm corr}$ related to the energy levels of the readout center. In order to discuss the effect of the model parameters on the spectral line shapes, it is required to know how much each SDR pair contributes to the detected SDR signal as a function of the pair separation distance.

Among all the readout centers interacting with a donor, we assume that the closest one exclusively forms the most efficient recombination pair. Then, in the ensemble measurement, each donor has a different separation r to the nearest readout center and, therefore, a different recombination time in the anti-parallel spin configuration, τ_{ap}. However τ_{ap} is much shorter than the pair creation time τ_{ec}, i. e., $\tau_{ap} \ll \tau_{ec} \ll \tau_p$, the signal intensity from a single D-R pair is determined by the electron capture time τ_{ec} and thus independent of r in cw SDR measurements. Then, the total intensity from an ensemble of D-R pairs should be determined directly by the

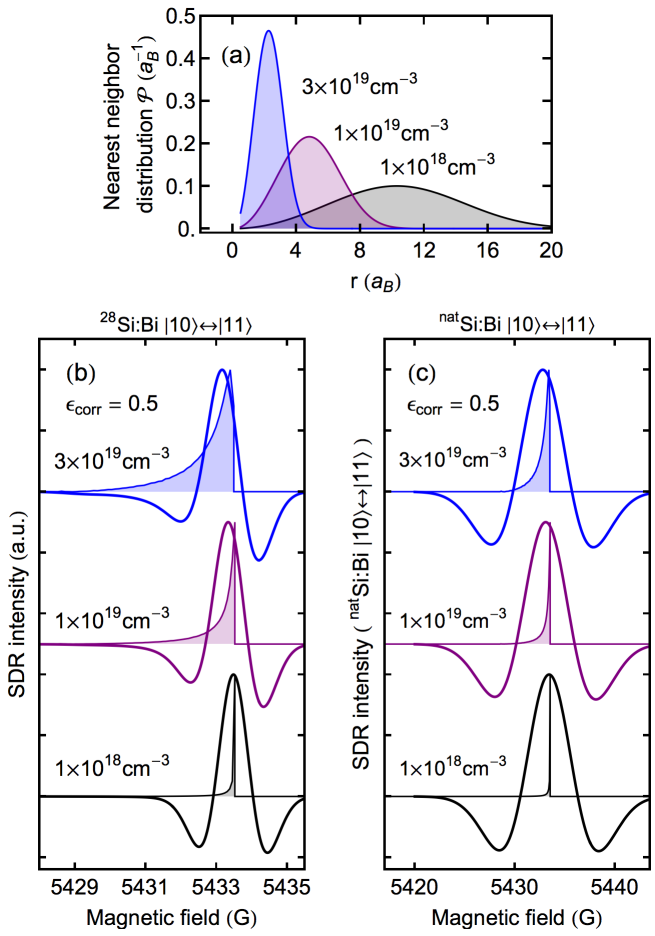

FIG. 4. (Color online.) (a) Distributions of the separation r between the donor and its nearest readout center for various concentrations N_R. (b, c) Simulated distributions of the $|10\rangle \leftrightarrow |11\rangle$ transition taking into account only the SDR pair distribution (thin filled lines) and its convolution with the second derivative of a Gaussian (thick lines) for ^{28}Si:Bi (b) and ^{nat}Si:Bi (c). The donor and readout center pair with the small enough separation r have strong interaction and thus contribute to the low-field tail in the distribution of resonant magnetic fields (thin solid lines). The FWHMs of the HCT_{9-12} lines are 6.7 G for ^{nat}Si:Bi (c) and 1.3 G for ^{28}Si:Bi (f), each of which is obtained from the width parameter of the 2nd derivative of a Gaussian function fitted to the HCT line (red curves). Due to such linewidth difference, the shift of the peak position to low field is much larger in ^{nat}Si:Bi (larger field scale), while the degree of line shape asymmetry is more apparent in ^{28}Si:Bi, as N_R is increased.

distribution function of the D-R separation r. Here we identify the concentration of the pair having the pair separation r as follows.

First, we assume that the SDR intensity is proportional to the probability $\mathcal{P}(r)\,dr$ of a Bi donor to find the nearest readout center at a distance between r and $r + dr$. This distribution can be written as[39]

$$\mathcal{P} = \frac{3}{\langle r_{RR}\rangle}\left(\frac{r}{\langle r_{RR}\rangle}\right)^2 \exp\left(-\frac{r^3}{\langle r_{RR}\rangle^3}\right) \qquad (8)$$

where $\langle r_{RR}\rangle = (3V/4\pi N_R)^{1/3}$ is the average distance between the readout center and its nearest neighbor. Such distributions are plotted in Fig. 4(a), as a function of r in the unit of a_B, for three different concentrations N_R of the readout centers. By combining Eq. (8) with the dependence of the hyperfine A on the D-R separation r obtained in section III B, the distribution in resonant magnetic field for the transition $|10\rangle \leftrightarrow |11\rangle$ is calculated and shown by thin curves in Figs. 4 (b, c). Since the peak for each r should be accompanied by a symmetric broadening due to inhomogeneous distribution of ^{29}Si nuclear spins in ^{nat}Si:Bi and of other Bi-donor and readout-center electron spins in ^{28}Si:Bi [as observed in Figs. 1(c) and 1(f)], the thin curves are convoluted with the second derivative of a Gaussian function to simulate the SDR spectra. The simulated spectra are shown as the thick curves in the same figures.

The mixing of atomic orbitals in the present model is assumed to be driven by the long range Coulomb potential of the ionized donor, and the readout center en-

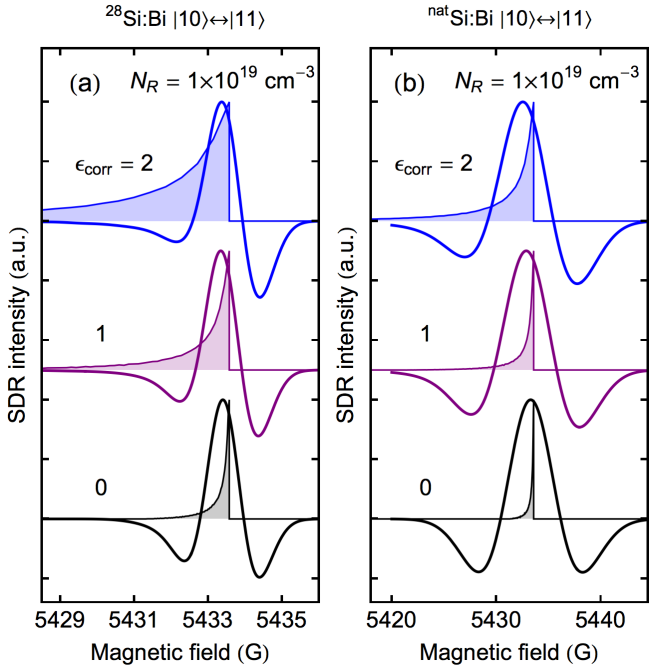

FIG. 5. (Color online.) Simulated distribution of the $|10\rangle \leftrightarrow |11\rangle$ transition in ^{28}Si:Bi (a) and ^{nat}Si:Bi (b) taking into account only the SDR pair distribution (thin lines) and its convolution with the second derivative of a Gaussian (thick lines) for various two-electron correlation parameters ϵ_{corr}. A larger ϵ_{corr} decreases the hyperfine interaction more in the anti-parallel spin pair configuration, which in turns broadens the distribution of the resonant magnetic field toward low field. The same procedure as for Fig. 4 was used for these simulations.

ergy E_{R} is set at -0.55 eV from the silicon conduction band. The remaining parameter of this model is the two-electron correlation parameter $\epsilon_{\rm corr}$ defined in section III A. It characterizes the mixing of the two-electron molecular orbitals in the spin singlet configuration Ψ_{+}. The dependence on $\epsilon_{\rm corr}$ of the resonant magnetic field is plotted in Fig. 5 for the $|10\rangle \leftrightarrow |11\rangle$ transition.

IV. COMPARISON OF EXPERIMENTAL RESULTS AND SIMULATIONS

A. Line position

At low magnetic field that we employed, the line positions are determined by the two parameters, g_{D} and A. In section III, we have shown the dependence of the resonant field on the electron density at the donor nucleus, ρ, through the hyperfine interaction. The donor electron g-factor further influences the line positions through both the Zeeman and the hyperfine [Eq. (5)] interactions. Because the resonant magnetic field of the HCT_{9-12} is robust against fluctuations in hyperfine A, it allows a precise determination of the g-factor of the donor electron. We measured an effective shift in the donor electron g-factor of +29 ppm in ^{28}Si:Bi (see Table I), which can be qualitatively explained by the second order perturbation theory as follows. For a donor electron non interacting with any readout center, the deviation δg_{D}^{∞} from the free electron g-factor resulting from the spin-orbit coupling is given by:

$$\delta g_{D}^{\infty}\mu_{B}B_{z}S_{z} = \sum_{n\neq\chi_{D}^{\infty}} \frac{\left\langle \chi_{D}^{\infty}\left|\mathcal{H}_{2}\right|n\right\rangle \left\langle n\left|\mathcal{H}_{2}\right|\chi_{D}^{\infty}\right\rangle}{E_{\chi_{D}^{\infty}} - E_{n}} \qquad (9)$$

where E_{n} are eigenvalues of the Hamiltonian $\mathcal{H}_{0}$ and $\mathcal{H}_{2} = g_{\rm fe}\mu_{B}\,\boldsymbol{S}\cdot\boldsymbol{B} - \lambda\,\boldsymbol{S}\cdot\boldsymbol{l} + \mu_{B}\,\boldsymbol{l}\cdot\boldsymbol{B}$ with $g_{\rm fe}$ the free electron g-factor, and λ the spin-orbit coupling parameter. Here the electron ground state $\left|\chi_{D}^{\infty}\right\rangle$ is an eigenstate of $\mathcal{H}_{0}$, neglecting the readout center potential V_{R}^{*}. However, as shown in section III A, the electron wave function is modified due to the presence of the readout center. Therefore, the g-factor correction of the donor electron in an SDR pair is $\delta g_{D} \approx a_{1}^{2}\delta g_{D}^{\infty} + a_{2}^{2}\delta g_{R}^{\infty}$ where δg_{D}^{∞} and δg_{R}^{∞} are the spin-orbit corrections of the isolated donor and readout center, respectively, and $a_{1,2}$ are defined in section III A. Since the g-factor of the isolated readout center $g_{R}^{\infty} = 2.005(3)$ (Ref. 19) is larger than the g-factor of the isolated donor $g_{D}^{\infty} = 2.00032$ (see Table I), the weighted average g_{D} must satisfy $g_{D}^{\infty} < g_{D} < g_{R}^{\infty}$. This qualitatively explains the larger effective g-factor of the donor in an SDR pair $g_{D} = 2.00038(2)$. Moreover, since the hyperfine interaction is proportional to the donor g-factor [Eq. (5)], the positive change of +29 ppm in g-factor measured in the SDR spectroscopy of ^{28}Si:Bi can be partly accounted for by the increase in effective hyperfine interaction of +84 ppm. On the other hand, the linewidth of a transition in $^{\rm nat}$Si:Bi is much larger than in ^{28}Si:Bi due to the inhomogeneous hyperfine interaction with the ^{29}Si nuclear spins. Therefore, the line position where the SDR intensity has a maximum, is shifted toward the mean of the resonant field distribution, away from its maximum (see Fig. 4 and 5). Thus, the decrease in effective hyperfine of -240 ppm for $^{\rm nat}$Si:Bi is attributed to a combination of the line asymmetry from the distribution in resonant magnetic field and of the broad linewidth from the inhomogeneous broadening.

The excitation frequency of the HCT_{9-12} (Fig. 1) has been determined using the reference values of the donor electron g-factor $g_{e}^{\rm EPR}$ (Table I). However, the $g_{e}^{\rm SDR}$ measured by SDR spectroscopy is different from $g_{e}^{\rm EPR}$. The resulting deviations in resonant field $\mathrm{HCT}_{9-12}^{\rm EPR} - \mathrm{HCT}_{9-12}^{\rm SDR}$ are +0.11 G for ^{28}Si:Bi and +0.35 G for $^{\rm nat}$Si:Bi. As a consequence, the spectra of Figs. 1(b) and 1(e) are not exactly at the $\mathrm{HCT}_{9-12}^{\rm SDR}$, and the sensitivity $\delta B_{z}/\delta A(B_{z} = B_{\rm HCT}^{\rm EPR})$ is finite: $+3\times10^{-8}$ G/MHz for ^{28}Si:Bi and $+8\times10^{-8}$ G/MHz for $^{\rm nat}$Si:Bi. Nevertheless, the line broadening due to these finite sensitivities is much smaller than the magnetic field inhomogeneity and cannot be detected.

B. Line shape

The experimental and simulated line shapes can be quantitatively compared in terms of moments m_{n} defined as:

$$m_{n} = \int (B - \langle B\rangle)^{n}\,\mathcal{I}(B)\,dB \qquad (10)$$

where $\mathcal{I}$ is the normalized signal intensity and $\langle B\rangle$ is the mean field for this spectrum. The degree of broadening and asymmetry can be represented by the variance m_{2} and skewness $\gamma_{1} = m_{3}/m_{2}^{3/2}$. The simulated values of m_{2} and γ_{1} for ^{28}Si:Bi are plotted as functions of N_{R} and $\epsilon_{\rm corr}$ in Figs. 6(a) and 6(b), respectively. The experimental variance and skewness are, $m_{2} = 0.62(5)$ G^{2} and $\gamma_{1} = -2.0(4)$ for the spin transition $|10\rangle \leftrightarrow |11\rangle$ in ^{28}Si:Bi. These are represented by the red surfaces in Figs. 6(a) and 6(b). The experimental uncertainties come mainly from a large background after the double-integration of the SDR signal, which is recorded as the second derivative of the sample photoconductivity, necessary for the intensity in Eq. (10) to evaluate the moments. The intersection in Fig. 6(c) represents the corresponding values for the correlation parameter and the readout center concentration: $\epsilon_{\rm corr} = 1$ and $N_{R} = 2\times10^{19}$ cm^{-3}. Such a high readout center concentration is consistent with the high damage cross-section for energetic bismuth ions and the limited recovery of the crystallinity by the annealing process. The two-electron correlation parameter $\epsilon_{\rm corr} = 1$ obtained in this study is equal to the one estimated for ^{31}P-P_{b0} ($\epsilon_{\rm corr} \approx 1.0$, Ref. 40), which confirms the localized wave function of the readout center.

For these numerical simulations, we used the experimental linewidth of ^{28}Si:Bi (1.3 G) measured at HCT_{9-12}. This rather large linewidth can be explained by the dipole-dipole interaction of the donor and the readout center electron spins for a concentration $N_R \approx 5 \times 10^{18}$ cm^{-3}. Moreover, one can expect a spectral line broadening due to the distribution in the donor electron g-factor. Assuming that this distribution covers a range

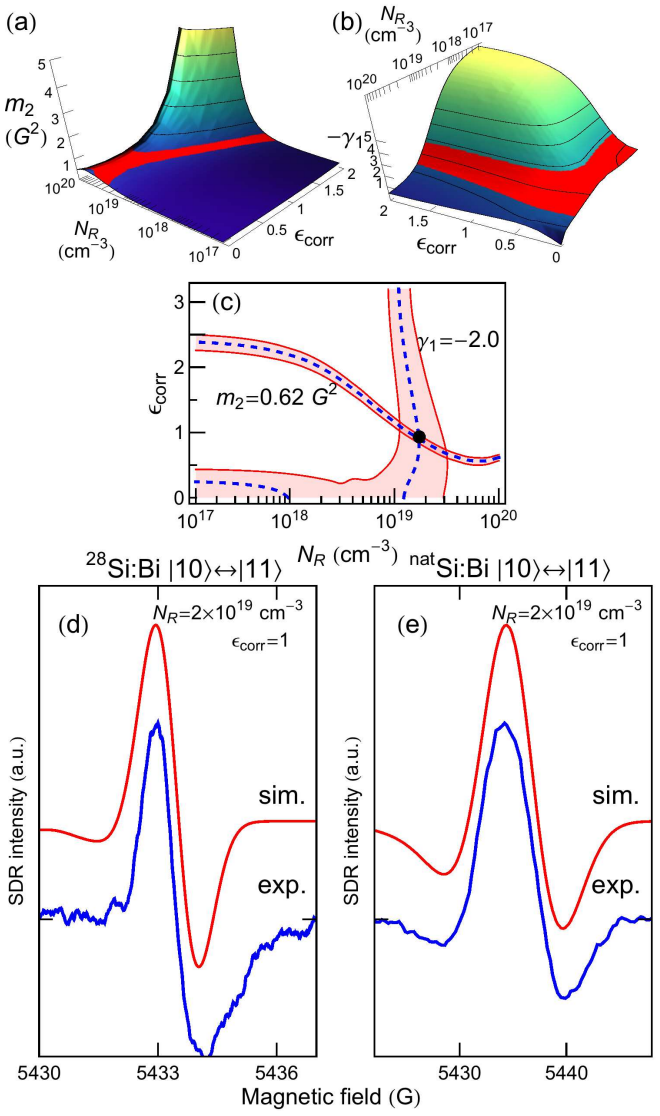

FIG. 6. (Color online.) Second (a) and third (b) standardized moments (m_2 and γ_1) of the simulated fractional change in the photoconductivity for the transition $|10\rangle \leftrightarrow |11\rangle$. The simulation was performed for ^{28}Si:Bi using the same 1.35 G linewidth as for Fig. 4(b) and 5(a). The red regions in the both plots represent the experimental values of m_2 and γ_1 and their uncertainty. These two regions are superposed in (c). The intersection of the $m_2 = 0.62$ G^2 and $\gamma_1 = 2.0$ is shown by a filled circle. The simulated line shapes for the pinpointed parameters in (c) of ^{nat}Si:Bi and ^{28}Si:Bi are shown in (d) and (e) (red lines), and compared to the experimental data (blue lines).

of ±93 ppm around $g_D = 2.00049$ for ^{nat}Si:Bi (see Table I), the broadening in the line FWHM, induced by the finite sensitivity $|\delta B_z/\delta g_e|$ (see Table II) at the HCT, should be +0.3 G. As a consequence, the distribution in the donor electron g-factor is negligible for ^{nat}Si:Bi and the FWHM linewidth of the Gaussian for the transition $|10\rangle \leftrightarrow |11\rangle$ is 5.7 G. For ^{28}Si:Bi however, even a smaller distribution of +29 ppm in g-factor is responsible for 0.1 G linewidth broadening (more than 10% of the linewidth measured at the HCT_{9-12}). The 0.1 G contribution of the g-factor distribution to the linewidth is multiplied by the sensitivity ratio $(\delta B_z/\delta g_e)_{|10\rangle\leftrightarrow|11\rangle} / (\delta B_z/\delta g_e)_{HCT} = 1.5$. Thus, the Gaussian linewidth to be used in the simulations for ^{28}Si:Bi is 1.35 G. It can be noted that for close pairs ($r < 1\, a_B$), the strong exchange interaction[34] can be neglected since the corresponding SDR intensity for $N_R = 2 \times 10^{19}$ cm^{-3} is below 0.1 % of the total SDR intensity. The above mentioned linewidths together with the N_R and ϵ_{corr} parameters calculated for ^{28}Si:Bi lead to the simulated spectra shown in Fig. 6(d) for ^{28}Si:Bi and (e) for ^{nat}Si:Bi. The experimental spectra are also shown below the simulations. The line shapes of the transition $|10\rangle \leftrightarrow |11\rangle$ for both ^{28}Si:Bi and ^{nat}Si:Bi samples are well reproduced. This demonstrates the validity of the presented molecular model for the SDR detection of donors for a wide range of host isotope composition.

Before concluding this section, we would like to point out the work of Morishita *et al.*[41] in which the spectroscopy of ^{28}Si:P was performed using low-field electrically detected magnetic resonance (LFEDMR), a technique similar to SDR. In this work, the authors compared the linewidth of ^{28}Si:P probed by LFEDMR at 160 MHz and by EPR at 9 GHz. No difference in the linewidth (0.1 G) for the $|2\rangle \leftrightarrow |3\rangle$ transition was observed and the authors concluded that the interaction of the phosphorus donor with the readout center is strong enough to allow the recombination process, but weak enough not to alter the transition linewidth. Yet, the hyperfine structure of the phosphorus donor is only 117 MHz so that its maximum change due to the interaction with the readout center is ∼ 13 times smaller for phosphorus than for bismuth. Moreover, the small phosphorus nuclear spin $I = 1/2$ makes the sensitivity $\delta B_z/\delta A$ relatively small: −0.10 G/MHz at 160 MHz for the $|2\rangle \leftrightarrow |3\rangle$. Thus, the effect of the phosphorus donor interaction with its readout center on the magnetic resonance is below the detection limit and the conclusions of Morishita do not contradict the present analysis.

V. HYPERFINE CLOCK TRANSITIONS FOR OTHER GROUP-V DONORS IN SILICON

There is no HCT in the EPR transitions of phosphorus donors in silicon. Other group-V donors have $I - 1/2$ HCT. At such points, as discussed in section IV A, the contribution of the g-factor distribution to the linewidth can be evaluated knowing the intrinsic EPR linewidth

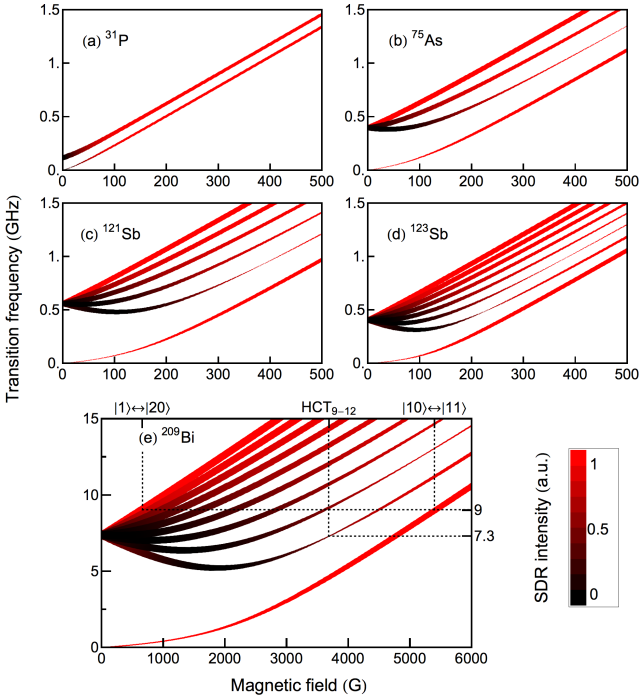

FIG. 7. (Color online.) EPR transition frequencies of group-V donors in silicon, (a) ^{31}P, (b) ^{75}As, (c) ^{121}Sb, (d) ^{123}Sb and (e) ^{209}Bi. The line thickness is proportional to the absolute $|\partial\nu/\partial A|$ value. The color represents the expected SDR intensity for a conventional continuous wave measurement. Our model shows that the SDR intensity of the HCT$_{9-12}$ line for Si:Bi is much weaker than the intensities for the X-band $|1\rangle \leftrightarrow |20\rangle$ and $|10\rangle \leftrightarrow |11\rangle$ lines. This was observed experimentally in Fig. 1. The frequency scale for ^{209}Bi is ten times larger than the others.

and extrapolated for an arbitrary transition. In fact, since the broadening due to the distribution in hyperfine (electron density at the donor nucleus) scales with $|\partial\nu/\partial A|$, the contribution to the linewidth calculated in this paper can be extrapolated for any points. The values of $|\partial\nu/\partial A|$ for EPR-allowed transitions of group-V donors in silicon (^{31}P, ^{75}As, ^{121}Sb, ^{123}Sb and ^{209}Bi) are plotted as the line thickness in Fig. 7. One can notice that for a given EPR transition, the high-field limit of $\partial\nu/\partial A$ is exactly m_I and, as a consequence, the field sensitivity to the hyperfine interaction is simply written as

$$\frac{\delta B_z}{\delta A} = \frac{h}{g_e\,\mu_e} m_I. \tag{11}$$

Also no polarization of the donor spins is required for SDR spectroscopy; only parallel spin pairs remain in the steady state under illumination. However, at low magnetic field, the donor eigenstates are not pure spin states. Thus, for one transition, the fraction of parallel and antiparallel electron spins of an SDR pair modified by magnetic resonance depends on the magnetic field.[19] With such considerations taken into account, the simulated SDR signal intensity for cw-SDR spectroscopy is plotted by the color scale in Fig. 7.

VI. SUMMARY AND CONCLUSIONS

In summary, we have performed the cw SDR spectroscopy of ^{28}Si:Bi and ^{nat}Si:Bi at 9 and 7 GHz and observed a significant SDR line narrowing at the HCT. The theoretical model proposed in this study for the SDR pair electron distribution reproduces the experimentally obtained line shapes very well. By analyzing the line shape at the HCT, we have shown that the main broadening process in ^{28}Si:Bi is the dipole-dipole interaction between the bismuth donor and the surrounding readout centers. Our results illustrate fundamental properties of hyperfine clock transitions and serve as a stepping stone for further investigations of coupling between microwave circuits and donors in silicon.

ACKNOWLEDGMENTS

The authors wish to express their appreciation to Martin S. Brandt, Felix Hoehne, and David Franke for fruitful discussions. This work has been supported in part by the JSPS Core-to-Core program, in part by MEXT, and in part by FIRST. S.Berger was supported by a JSPS Fellowship for his stay at Keio University. We also acknowledge the Australian Government's NCRIS/EIF programs for access to Heavy Ion accelerator Facilities at the Australian National University.

[1] M. H. Devoret and R. J. Schoelkopf, Science **339**, 1169 (2013).
[2] J. F. Cochran and D. E. Mapother, Phys. Rev. **111**, 133 (1958).
[3] G. Feher, Phys. Rev. **114**, 1219 (1959).
[4] I. Chiorescu, Y. Nakamura, C. Harmans, and J. E. Mooij, Science **299**, 1869 (2003).
[5] G. W. Morley, M. Warner, A. M. Stoneham, P. T. Greenland, J. van Tol, C. W. M. Kay, and G. Aeppli, Nat. Mater. **9**, 725 (2010).
[6] R. E. George, W. Witzel, H. Riemann, N. V. Abrosimov, N. Noetzel, M. L. W. Thewalt, and J. J. L. Morton, Phys. Rev. Lett. **105**, 067601 (2010).
[7] C. D. Weis, C. C. Lo, V. Lang, A. M. Tyryshkin, R. E. George, K. M. Yu, J. Bokor, S. A. Lyon, J. J. L. Morton, and T. Schenkel, Appl. Phys. Lett. **100**, 172104 (2012).
[8] M. Belli, M. Fanciulli, and N. V. Abrosimov, Phys. Rev. B **83**, 235204 (2011).

[9] G. Wolfowicz, S. Simmons, A. M. Tyryshkin, R. E. George, H. Riemann, N. V. Abrosimov, P. Becker, H. J. Pohl, S. A. Lyon, M. L. W. Thewalt, and J. J. L. Morton, Phys. Rev. B **86**, 245301 (2012).

[10] G. Wolfowicz, A. M. Tyryshkin, R. E. George, H. Riemann, N. V. Abrosimov, P. Becker, H. J. Pohl, M. L. W. Thewalt, S. A. Lyon, and J. J. L. Morton, Nat. Nanotechnol. **8**, 561 (2013).

[11] S. J. Balian, M. B. A. Kunze, M. H. Mohammady, G. W. Morley, W. M. Witzel, C. W. M. Kay, and T. S. Monteiro, Phys. Rev. B **86**, 104428 (2012).

[12] T. Sekiguchi, M. Steger, K. Saeedi, M. L. W. Thewalt, H. Riemann, N. V. Abrosimov, and N. Notzel, Phys. Rev. Lett. **104**, 137402 (2010).

[13] G. W. Morley, P. Lueders, M. H. Mohammady, S. J. Balian, G. Aeppli, C. W. M. Kay, W. M. Witzel, G. Jeschke, and T. S. Monteiro, Nat. Mater. **12**, 103 (2013).

[14] M. H. Mohammady, G. W. Morley, and T. S. Monteiro, Phys. Rev. Lett. **105**, 067602 (2010).

[15] E. Abe, A. M. Tyryshkin, S. Tojo, J. J. L. Morton, W. M. Witzel, A. Fujimoto, J. W. Ager, E. E. Haller, J. Isoya, S. A. Lyon, M. L. W. Thewalt, and K. M. Itoh, Phys. Rev. B **82**, 121201 (2010).

[16] W. M. Witzel, M. S. Carroll, A. Morello, L. Cywinski, and S. Das Sarma, Phys. Rev. Lett. **105**, 187602 (2010).

[17] A. M. Tyryshkin, S. Tojo, J. J. L. Morton, H. Riemann, N. V. Abrosimov, P. Becker, H. J. Pohl, T. Schenkel, M. L. W. Thewalt, K. M. Itoh, and S. A. Lyon, Nat. Mater. **11**, 143 (2012).

[18] M. Steger, K. Saeedi, M. L. W. Thewalt, J. J. L. Morton, H. Riemann, N. V. Abrosimov, P. Becker, and H. J. Pohl, Science **336**, 1280 (2012).

[19] P. A. Mortemousque, T. Sekiguchi, C. Culan, M. P. Vlasenko, R. G. Elliman, L. S. Vlasenko, and K. M. Itoh, Appl. Phys. Lett. **101**, 082409 (2012).

[20] D. J. Lepine, Phys. Rev. B **6**, 436 (1972).

[21] D. Vion, A. Aassime, A. Cottet, P. Joyez, H. Pothier, C. Urbina, D. Esteve, and M. H. Devoret, Science **296**, 886 (2002).

[22] H. Lyons, Ann. New York Acad. Sci **55**, 831 (1952).

[23] P. Kusch, Phys. Rev. **76**, 161 (1949).

[24] S. A. Diddams, T. Udem, J. C. Bergquist, E. A. Curtis, R. E. Drullinger, L. Hollberg, W. M. Itano, W. D. Lee, C. W. Oates, K. R. Vogel, and D. J. Wineland, Science **293**, 825 (2001).

[25] F. A. Trumbore, Bell Syst. Tech. **39**, 205 (1960).

[26] O. J. Marsh, R. Baron, G. A. Shifrin, and J. W. Mayer, Appl. Phys. Lett. **13**, 199 (1968).

[27] R. Baron, G. A. Shifrin, O. J. Marsh, and J. W. Mayer, J. Appl. Phys. **40**, 3702 (1969).

[28] J. P. de Souza and P. F. P. Fichtner, J. Appl. Phys. **74**, 119 (1993).

[29] E. Abramof, A. Ferreira da Silva, B. E. Sernelius, J. P. de Sousa, and H. Boudinov, Phys. Rev. B **55**, 9584 (1997).

[30] P. Studer, S. R. Schofield, C. F. Hirjibehedin, and N. J. Curson, Appl. Phys. Lett. **102**, 012107 (2013).

[31] F. Hoehne, L. Dreher, M. Suckert, D. P. Franke, M. Stutzmann, and M. S. Brandt, Phys. Rev. B **88**, 155301 (2013).

[32] R. T. Cox, D. Block, A. Herve, R. Picard, C. Santier, and R. Helbig, Solid State Commun. **25**, 77 (1978).

[33] J. M. Lu, F. Hoehne, A. R. Stegner, L. Dreher, M. Stutzmann, M. S. Brandt, and H. Huebl, Phys. Rev. B **83**, 235201 (2011).

[34] M. Suckert, F. Hoehne, L. Dreher, M. Kuenzl, H. Huebl, M. Stutzmann, and M. S. Brandt, Molecular Physics **111**, 2690 (2013).

[35] S. Kimura, H. Ono, T. Ikarashi, and T. Ishikawa, Jpn. J. Appl. Phys. Part 1 - Letters **32**, L1074 (1993).

[36] D. K. Wilson and G. Feher, Phys. Rev. **124**, 1068 (1961).

[37] L. Dreher, T. A. Hilker, A. Brandlmaier, S. T. B. Goennenwein, H. Huebl, M. Stutzmann, and M. S. Brandt, Phys. Rev. Lett. **106**, 037601 (2011).

[38] L. Dreher, Ph.D. thesis, Technische Universität München, 2013.

[39] P. Hertz, Math. Ann. **67**, 387 (1909).

[40] E. H. Poindexter, G. J. Gerardi, M. E. Rueckel, P. J. Caplan, N. M. Johnson, and D. K. Biegelsen, J. Appl. Phys. **56**, 2844 (1984).

[41] H. Morishita, E. Abe, W. Akhtar, L. S. Vlasenko, A. Fujimoto, K. Sawano, Y. Shiraki, L. Dreher, H. Riemann, N. V. Abrosimov, P. Becker, H. J. Pohl, M. L. W. Thewalt, M. S. Brandt, and K. M. Itoh, Appl. Phys. Express **4**, 021302 (2011).